

Ceria-Induced Strategy To Tailor Pt Atomic Clusters on Cobalt–Nickel Oxide and the Synergetic Effect for Superior Hydrogen Generation

Chongbei Wu,[†] Jifang Zhang,[†] Jingya Guo,[†] Linxin Sun,[†] Jun Ming,^{*,†,‡} Hailin Dong,[†] Yanchun Zhao,^{*,†} Jianniao Tian,[†] and Xiulin Yang^{*,†,‡}

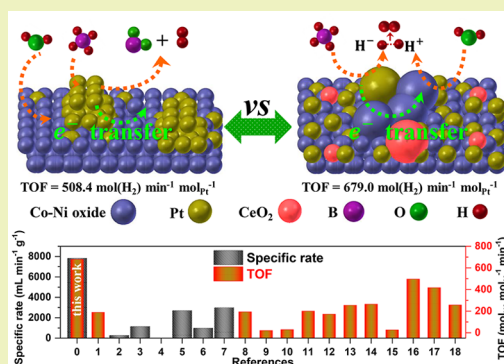
[†]Key Laboratory for the Chemistry and Molecular Engineering of Medicinal Resources (Ministry of Education of China), College of Chemistry and Pharmacy, Guangxi Normal University, Guilin 541004, People's Republic of China

[‡]State Key Laboratory of Rare Earth Resource Utilization, Changchun Institute of Applied Chemistry, Chinese Academy of Sciences, Changchun 130022, People's Republic of China

Supporting Information

ABSTRACT: A new and reusable hybrid catalyst of Pt/CeO₂–Co₇Ni₂O_x is fabricated readily, in which a high dispersion of Pt atomic cluster is successfully achieved by the introduction of CeO₂. The oxidation states of each elemental metal in varied compositions are studied systematically to design the catalyst. The optimal Pt/CeO₂–Co₇Ni₂O_x catalyst exhibits an extremely high specific H₂ evolution rate of 7834.8 mL_{H₂} min^{−1} g_{cat}^{−1} and turnover frequency of 679.0 mol_{H₂} min^{−1} mol_{Pt}^{−1} for the hydrolysis of alkalinized NaBH₄ solution. It is one of the most efficient catalysts so far, and the reason is ascribed to the lower activation energy (47.4 kJ mol^{−1}) as we confirmed. The lower energy barrier and high performances mainly results from the ultrasmall Pt atomic clusters, which have more active sites to adsorb and break the B–H bonds in BH₄[−] ions for the generation of negative charged H[−] via electron transfer, and then the H[−] can immediately combine with the positive charged H⁺ (originated from the weakened H–O–H bond on the Ce–Co–Ni oxide) to produce H₂ fast.

KEYWORDS: CeO₂, Pt-Alloy particles, Hydrolysis, Sodium borohydride, Reusability



INTRODUCTION

The conventional energy sources including the coal, oil, and natural gas are unable to meet the increased energy requirement currently,¹ and also the reaction byproducts (e.g., CO₂, nitrous oxides, sulfur oxides) can lead to a serious environmental pollutions (e.g., greenhouse effect, acid rain, etc.) which cannot satisfy the sustainability request.² Thus, it is urgent to explore an alternative to replace the fossil fuels. Recently, hydrogen (H₂) has attracted great attention due to the higher energy density (ca. 3 times higher than that of conventional oil) and zero-elimination after the use (e.g., only the nonpolluted water formed).³ Though the storage and transportation of H₂ under a high pressure in a safe manner is still challenging. Alternatively, the hydrogen can be stored and transported safely as hydrogen atoms in chemical materials (e.g., NaBH₄, NH₃BH₃, etc.).^{4,5} The materials of metal hydride, boron hydride, amides, borane ammonia, and formic acid are well-known candidates for this issue as reported.^{6–8} Note that the features of sodium borohydride (NaBH₄) including the high hydrogen storage capacity (10.8 wt %) and easy separation of H₂ from the products (NaBH₄ + 2H₂O → NaBO₂ + 4H₂) enable it to be very attractive.^{9–12} However, explore a highly

efficient catalysts to activate the H atoms in the NaBH₄ is still challenging.

To date, most transitional elements have been explored as potential catalysts for the catalytic hydrolysis of NaBH₄,^{13–15} because the non-noble metal-based catalysts (e.g., Fe, Co, Ni, etc.) are considered to be the most promising candidates; but, the low activities and inferior cycle stability hinder their development seriously.^{16–23} By contrast, the precious metal based catalysts (e.g., Pt, Pd, and Ru) exhibit an excellent catalytic activity, but the high cost cannot meet the huge demand in industrial production. To overcome these disadvantages, the noble/non-noble based hybrid catalysts were developed,²⁴ which can largely decrease the noble metal amount and get a relatively high catalytic activities. As a result, the hybrid catalysts of Pt/3D SiC,²⁵ Pt/SiO₂,²⁶ Pt/Co₃O₄,²⁷ Pt/LiCoO₂,²⁸ Ni–Ru,²⁹ Co_{0.8}–Ag_{0.2}–B,³⁰ Ni/Au/Co,³¹ Ni_{0.9}Pt_{0.1}/Ce₂O₃,³² and Rh/Ni BNPs,³³ have been widely reported, but the performances in terms of specific H₂

Received: January 5, 2018

Revised: April 11, 2018

Published: April 29, 2018

evolution rates, turnover frequency values, and long-term reusability still have a large space to be enhanced.

Herein, a new hybrid catalyst of Pt/CeO₂-Co₇Ni₂O_x is reported, in which the CeO₂ is introduced to tailor the Pt atomic clusters on Co-Ni oxide support for a fine dispersion and higher catalytic performance. Besides, the effect of Co/Ni ratio and the role of CeO₂ were studied in detail. Our designated Pt/CeO₂-Co₇Ni₂O_x hybrid catalyst exhibits excellent catalytic ability for hydrolysis of alkalized NaBH₄ solution, in which a faster specific H₂ evolution rate, higher TOF value, and longer time reusability are obtained. A catalytic mechanism model on the Pt/CeO₂-Co₇Ni₂O_x hybrid catalyst is presented to interpret the higher performances.

EXPERIMENTAL SECTION

Catalysts Preparation. All chemical reagents are analytical grade and used without further purification. The hybrid Pt/CeO₂-Co₇Ni₂O_x catalyst was prepared by a one-pot reduction method. Typically, 83.3 mg of CoCl₂·6H₂O (0.35 mM), 23.7 mg of NiCl₂·6H₂O (0.1 mM), 35.5 mg of Ce(NO₃)₃·6H₂O, and 2.78 mL of H₂PtCl₆ (3.7 wt %) were dissolved in 60 mL of water containing 109.8 mg of hexadecyl trimethylammonium bromide (CTAB). The solution was ultrasonicated for 10 min first and then kept with magnetic stirring for 2 h. Afterward, 10 mL of fresh aqueous NaBH₄ with the concentration of 10 mg mL⁻¹ was added into the above solution under stirring, and the lathers were removed by spraying 10 mL of ethanol as the antifoaming agent. After the reaction for 20 min, the black samples was collected and washed by H₂O and C₂H₅OH several times, and finally it was freeze-dried at -50 °C for overnight. The as-prepared sample was named as Pt/CeO₂-Co₇Ni₂O_x (Figure S1). Using the same procedures, the molar ratio of Co/Ni in Pt/CeO₂-Co_mNi_nO_x (*m* + *n* = 9) were prepared to search an optimal value, in which the theoretical mass loading of Pt were fixed at 20 wt % in the total mass of metal. Besides, different loading of Pt was further optimized on the selected CeO₂-Co₇Ni₂O_x composite. The Pt particles supported on the commercial XC-72 carbon (20 wt %) were also prepared using NaBH₄ as the reducing agent directly for the comparison.

Catalyst Characterizations. The morphologies and microstructures of the catalysts were characterized by scanning electron microscopy (SEM, FEI Quanta 200 FEG) with X-ray energy dispersive spectrometry (EDS) and transmission electron microscopy (TEM, JEM-2100F). The crystalline information on catalysts was analyzed by X-ray powder diffraction (XRD, Rigaku D/Max 2500 V/PC) with a sweep speed for 2.0° min⁻¹. The X-ray photoelectron spectrometer (XPS, JPS-9010 Mg K α) was used to analyze the chemical states of different elements. The actual loadings of different metals in the catalyst were checked by inductive coupled plasma atomic emission spectroscopy (ICP-AES, IRIS Intrepid II XSP).

Catalytic Measurements. The catalytic activities, reusability, and activation energy of as-prepared catalysts for H₂ evolution of NaBH₄ hydrolysis were analyzed as follows. In detail, 50 mL of 150 mM aqueous solution of NaBH₄ containing 0.4 wt % NaOH was injected into a round-bottomed flask (100 mL) and stirred for 0.5 h at 298 K in a water bath. 10 mg of catalyst was added into the above solution, and the generated H₂ was elevated by a drainage method, in which the overflowed water was collected and weighted by a balance. The reusability procedures of the catalyst were described as below. The above hydrolyzed solution of NaBH₄ was stirred for another 1.0 h for the completed reaction in the first-cycle, and then the catalytic procedure of NaBH₄ hydrolysis was repeated and detected the H₂ generation again using the same amount of NaBH₄. The activation energy of the hybrid catalyst was evaluated in the same system under the different temperatures of 298, 303, 308, 313, and 318 K. The hydrogen generation rate (HGR) and turnover frequency (TOF) values are calculated as follows:^{25,34} HGR = $V_{\text{H}_2\text{O}}/(m_{\text{total}} \times t)$ and TOF = $n_{\text{H}_2}/(n_{\text{Pt}} \times t)$, where $V_{\text{H}_2\text{O}}$ is the volume of drained water (mL), m_{total} is the total mass of the hybrid catalyst (g), n_{H_2} is the moles

of generated H₂, n_{Pt} is the moles of Pt in the hybrid catalyst, and t is the total reaction time (min).

RESULTS AND DISCUSSION

Structural Features of CeO₂-Induced Catalyst. A comparative X-ray diffraction patterns (XRD) patterns of CeO₂-tuned Pt/Co₇Ni₂O_x and Pt/Co₇Ni₂O_x hybrid catalyst is shown in Figure 1a. The indexed peaks at 40.3, 46.8, and 68.8°

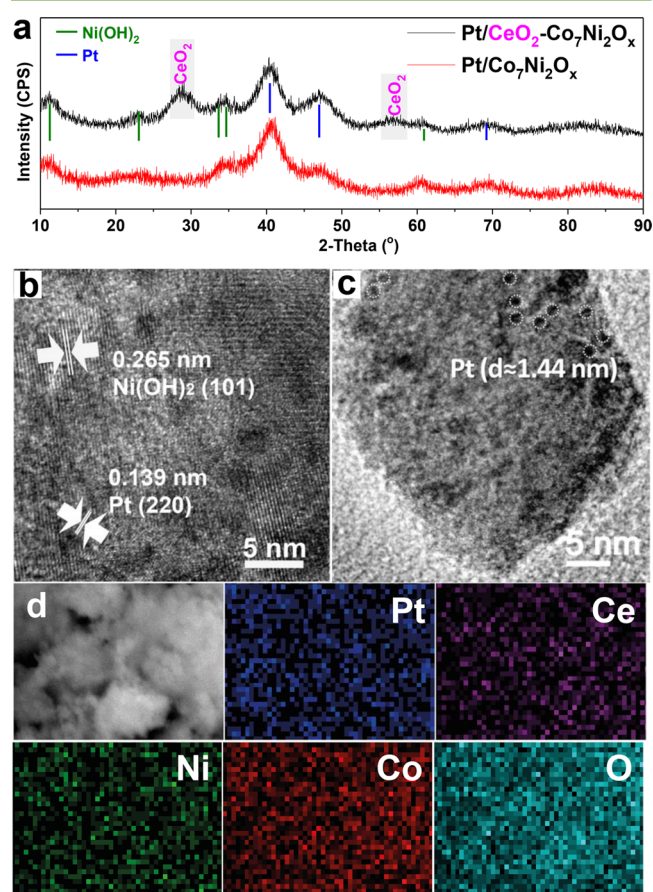


Figure 1. (a) XRD patterns of the synthesized Pt/CeO₂-Co₇Ni₂O_x and Pt/Co₇Ni₂O_x composites. (b) High-resolution TEM image of the Pt/Co₇Ni₂O_x. (c) High-resolution TEM image of the Pt/CeO₂-Co₇Ni₂O_x. (d) EDS mapping of the Pt/CeO₂-Co₇Ni₂O_x with Pt, Ce, Ni, Co, and O, respectively.

were ascribed to the face-centered cubic structure of metal Pt (JCPDS: 04-0802),³⁵ whereas the peaks located at ca. 11.3°, 22.9°, 33.6°, 34.6°, and 61.0° demonstrate the existence of crystal Ni(OH)₂ (JCPDS: 38-0715). Importantly, two diffraction peaks at ca. 28.6 and 56.3° corresponding to the crystal facets (111) and (311) of CeO₂ (JCPDS: 34-0394)³⁶ appear on the CeO₂-tuned Pt/Co₇Ni₂O_x catalyst, indicating the CeO₂ was incorporated into the composite. Note that there is no diffraction peaks of Co species detected in the hybrid materials, indicating that amorphous form of Co species. Note that the diffraction peaks of Pt shifts positively comparing to the standard peaks of Pt, confirming the partial alloys of Pt and Ni/Co are formed in the catalysts. Moreover, it should be noted that no Pt-Ce alloy existed in the Pt/CeO₂ composite compare to the commercial Pt/C material (Figure S2).

The microstructural differences of Pt/Co₇Ni₂O_x and Pt/CeO₂-Co₇Ni₂O_x are further characterized. The Pt/Co₇Ni₂O_x

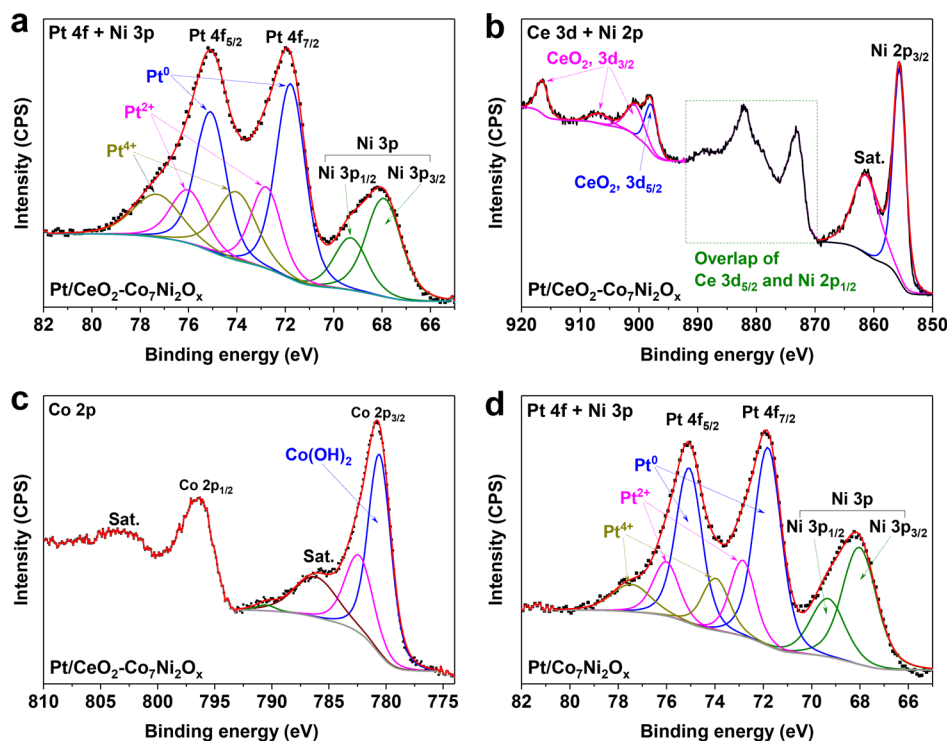


Figure 2. High-resolution XPS spectra of (a) Pt 4f + Ni 3p, (b) Ce 3d + Ni 2p, and (c) Co 2p for Pt/CeO₂-Co₇Ni₂O_x. (d) High-resolution XPS spectra of Pt 4f + Ni 3p from Pt/Co₇Ni₂O_x.

catalyst consists of lots of larger particles, where the Pt aggregated particles are dispersed randomly on the surface of the Co₇Ni₂O_x composite, as shown in Figure S3. By contrast, the Pt/CeO₂-Co₇Ni₂O_x catalyst presents particulate structures and they interconnect each other regularly after the introduction of CeO₂ (Figure S4). Another salient different is the distribution of Pt-alloy atomic clusters, which are intertwined with the support of Co₇Ni₂O_x, as confirmed by the different lattice spaces of ca. 0.265 and 0.139 nm ascribed to the crystal facets of Ni(OH)₂ (101) and Pt (220) (Figure 1b). Alternatively, the Pt-alloy atomic clusters have a high distribution around at ca. 1.44 nm on the CeO₂-Co₇Ni₂O_x surface, which is significantly smaller than the Pt alloy clusters on Co₇Ni₂O_x support (Figure S5). Besides, the fine distribution of Pt-alloy atomic clusters on the skeleton structures of CeO₂-Co₇Ni₂O_x is further confirmed by TEM image (Figure 1c), in which the lattice spacing of the Pt atomic clusters is almost undetectable. The energy dispersive spectroscopy (EDS) reveals again that the elements of Pt, Ce, Co, Ni, and O in the Pt/CeO₂-Co₇Ni₂O_x are uniformly distributed (Figure 1d, Figure S6), in which the actual Pt loading in the composite is 10.05 wt % (Table S1).

Chemical States Analysis. To identify the elemental valence in the Pt/CeO₂-Co₇Ni₂O_x catalyst, the X-ray photoelectron spectroscopy (XPS) measurement was performed. The full-range XPS spectrum demonstrates the existence of Pt, Ce, Co, Ni, O, and C elements (Figure S7), which is consistent with the analysis of energy dispersive spectroscopy. Before analysis, the high-resolution C 1s spectrum is corrected for the spectrum, and it can be convoluted with three main peaks at C—C (284.8 eV), C—O (286.0 eV), and C=O (288.9 eV) (Figure S7).³⁷ First, the partially overlapped high-resolution Pt 4f and Ni 3p spectra in Figure 2a are convoluted into Pt 4f and Ni 3p regions, respectively. The main pair of asymmetric peaks

at 71.8 and 75.1 eV in Pt 4f region confirm the existence of metallic Pt⁰, whereas the peaks at 72.8 and 76.0 eV are attributed to Pt²⁺ species, and the peaks at 74.0 and 77.3 eV are related to Pt⁴⁺ species.^{38,39} In the Ni 3p region, it can be split into a pair of peaks with binding energies at 67.9 eV for Ni 3p_{3/2} and 69.3 eV for Ni 3p_{1/2}, which are consistent with the binding energies of Ni²⁺ in oxide or hydroxide,⁴⁰ as confirmed in XRD patterns (Figure 1a). In the Ce 3d + Ni 2p region as shown in Figure 2b, the binding energy at 897.9 eV is considered as Ce 3d_{5/2} of CeO₂, whereas the binding energies at 900.7, 906.7, and 916.5 eV are resulted from Ce 3d_{3/2} of CeO₂.⁴¹ In the subsequent Ni 2p region, the appearance of Ni 2p_{3/2} from Ni oxide or hydroxide at binding energy of 855.7 eV is consistent with the analyzed results of Ni 3p. Both results confirm the existence of CeO₂. In addition, the high-resolution Co 2p_{3/2} spectra with fitting peaks at 780.6, 782.4, 786.1, and 790.5 eV can be identified as Co(OH)₂ species (Figure 2c).^{42,43} As a comparison, the high-resolution Pt 4f + Ni 3p spectrum of Pt/Co₇Ni₂O_x catalyst is further analyzed in Figure 2d. The content of metallic Pt⁰ in Pt/Co₇Ni₂O_x (61.9%) is significantly higher than that in the Pt/CeO₂-Co₇Ni₂O_x (52.3%) hybrid material (Figure S8). This result indicates that the introduction of CeO₂ in the hybrid material can considerably increase the amount of oxidized Pt species (Table S2).

Catalytic Performance. The effect of Co/Ni molar ratio for the catalytic performance of CeO₂-tailored Pt-alloy atomic clusters on Co-Ni oxide support are studied for H₂ generation in 150 mM NaBH₄ at ~298 K (Figure S9). It is found that the hydrolysis performance gradually increases as increasing the Co amount (Figure 3a). The related specific H₂ evolution rates of catalyst with different Co/Ni ratio for hydrolysis of NaBH₄ solution is shown in Figure 3b. The designated Pt/CeO₂-Co₇Ni₂O_x hybrid catalyst shows the higher specific H₂ evolution rate of 7834.8 mL_{H2} min⁻¹ g_{cat}⁻¹, which is 4.95-

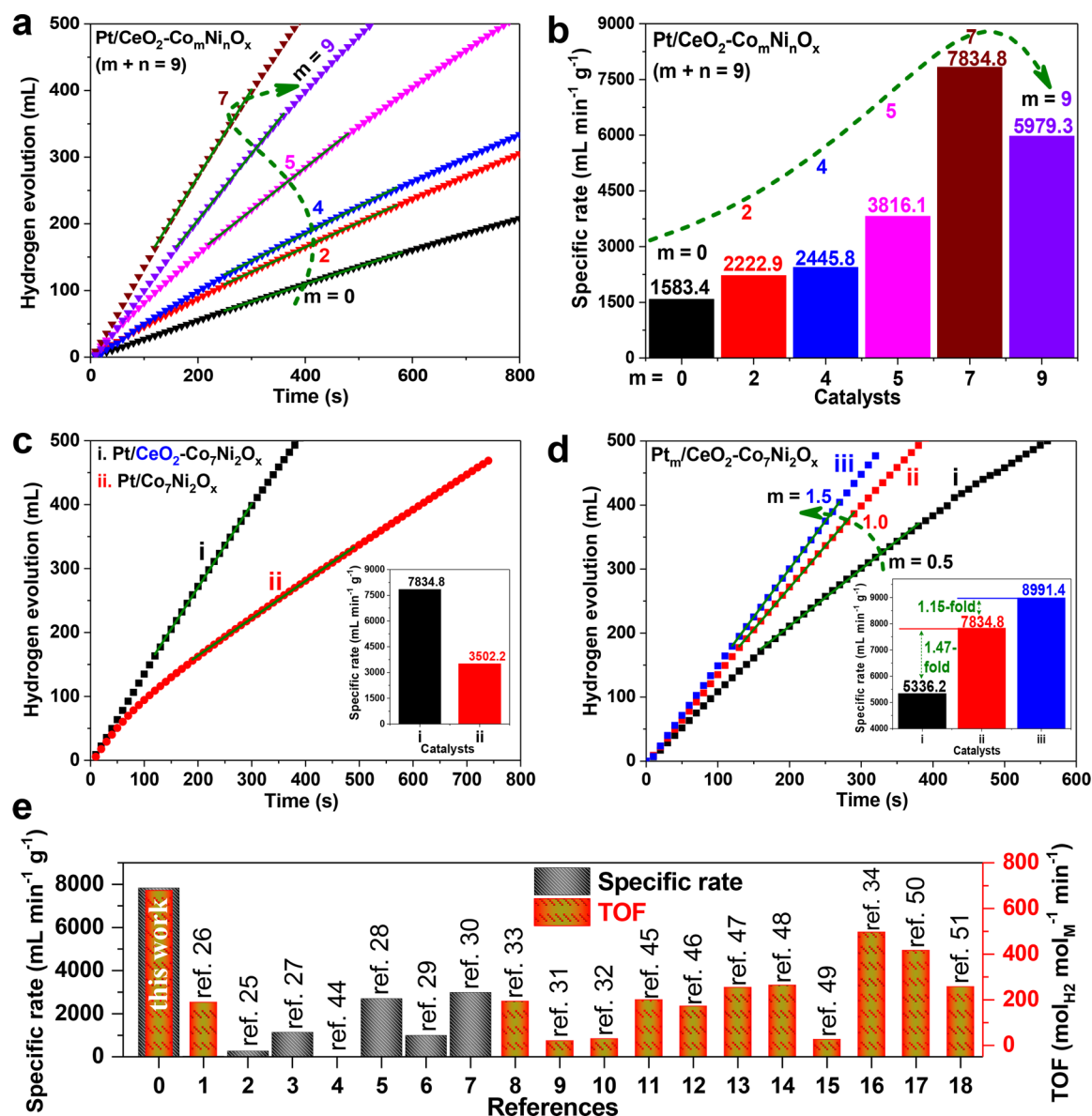


Figure 3. (a) Time dependent H₂ generation and corresponding (b) specific rates for H₂ evolution on different CeO₂ tuned Pt-alloy/Ce–Co–Ni hybrid catalysts for NaBH₄ hydrolysis. Time dependent H₂ generation on (c) Pt/CeO₂–Co₇Ni₂O_x and Pt/Co₇Ni₂O_x and (d) support of CeO₂–Co₇Ni₂O_x modified with different loadings of Pt for NaBH₄ hydrolysis. Insets are corresponding calculated specific rates for H₂ evolution. (e) Comparison of this work with ever reported literatures for H₂ generation.

and 1.31-fold higher than the Pt/CeO₂–Ni₉O_x and Pt/CeO₂–Co₉O_x catalysts, respectively. Besides, the Pt/CeO₂–Co₇Ni₂O_x catalyst has a high TOF value of 679.0 mol_{H₂} min⁻¹ mol_{Pt}⁻¹. These values are superior than 832.0 mL_{H₂} min⁻¹ g_{cat}⁻¹ and 31.5 mol_{H₂} min⁻¹ g_{Pt}⁻¹ of Pt/XC-72 (20 wt %) (Figure S10), fully demonstrating the positive effect of transition metal oxide in catalytic hydrolysis reaction. Besides, these values are also much higher than 3502.2 mL_{H₂} min⁻¹ g_{cat}⁻¹ and 508.4 mol_{H₂} min⁻¹ mol_{Pt}⁻¹ of Pt/Co₇Ni₂O_x without CeO₂ (Figure 3c). The enhanced capabilities should be ascribed to the smaller Pt clusters induced by CeO₂, in which the tiny crystals can bring more grain boundaries and active sites for the reactions. Thus, the Pt/CeO₂–Co₇Ni₂O_x hybrid catalyst demonstrates the higher catalytic activities and it indicates the existence of a significant synergistic effect. Additionally, it can find that single CoO_x, NiO_x, CeO₂, and CeO₂–Co₇Ni₂O_x particles almost do not have the capacity for hydrolysis of NaBH₄ (Figure S11).

Furthermore, we find that a higher Pt loading demonstrates a higher specific H₂ evolution rate, in which the specific H₂ evolution rate of Pt_{1.0}/CeO₂–Co₇Ni₂O_x increases 1.47-fold compared to that of Pt_{0.5}/CeO₂–Co₇Ni₂O_x, but the increment is only 1.15-fold when the Pt increases from Pt_{1.0}/CeO₂–Co₇Ni₂O_x to Pt_{1.5}/CeO₂–Co₇Ni₂O_x, as shown in Figure 3d. Thus, the utilization efficiency of Pt in Pt_{1.0}/CeO₂–Co₇Ni₂O_x hybrid catalyst is another feature for applications. Note that the catalytic activities of desingated Pt_{1.0}/CeO₂–Co₇Ni₂O_x are comparable and even superior than most results reported before (Figure 3e).^{25–34,44–51}

The advantages of CeO₂-tailored catalyst were further confirmed in its reusability. We find that the Pt/CeO₂–Co₇Ni₂O_x catalyst requires only about 6.6, 9.0, 9.7, 9.9, and 12.7 min to get 500 mL of H₂ for the consecutive five runs (Figure 4a), respectively. Specially, the special H₂ evolution rate is almost undetectable before conducting each recycle test

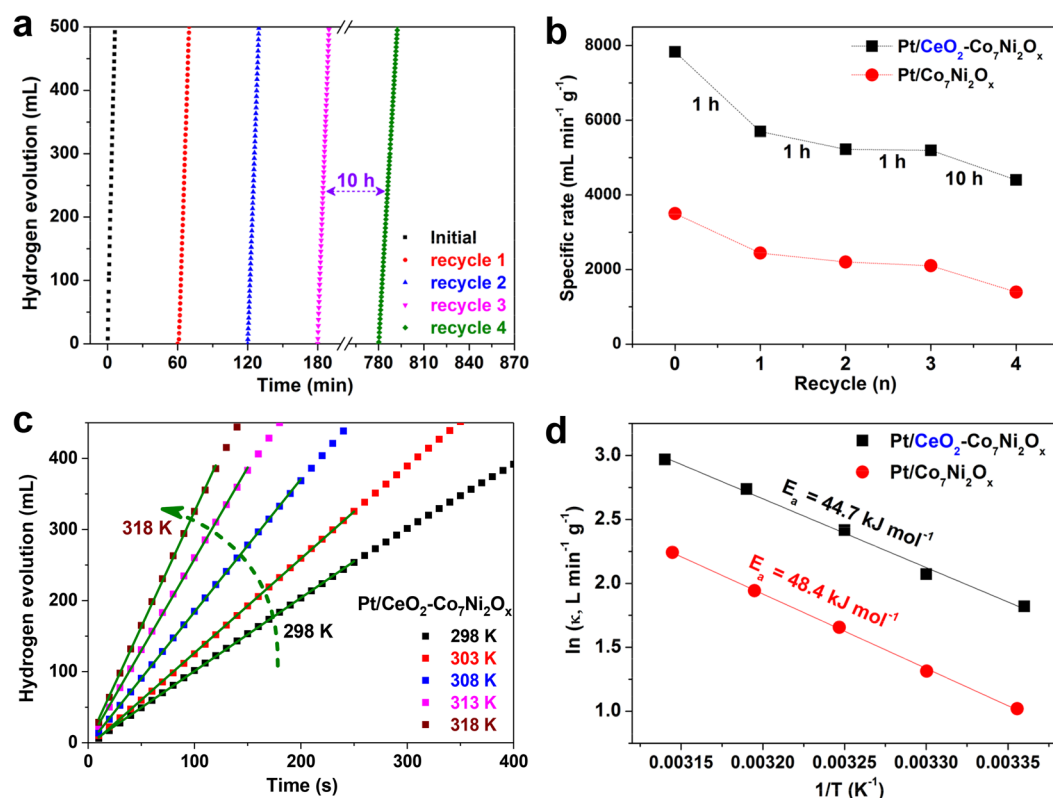


Figure 4. (a) Recycling stability test of the Pt/CeO₂-Co₇Ni₂O_x hybrid catalyst in 150 mM NaBH₄ + 0.4 wt % NaOH solution at ~298 K. (b) Summarized TOF values and specific H₂ evolution rates with different recycle times from panel a. (c) Temperatures effect on the designated Pt/CeO₂-Co₇Ni₂O_x hybrid catalyst for hydrolysis of NaBH₄ to H₂ production. (d) Arrhenius plots are derived from panel c.

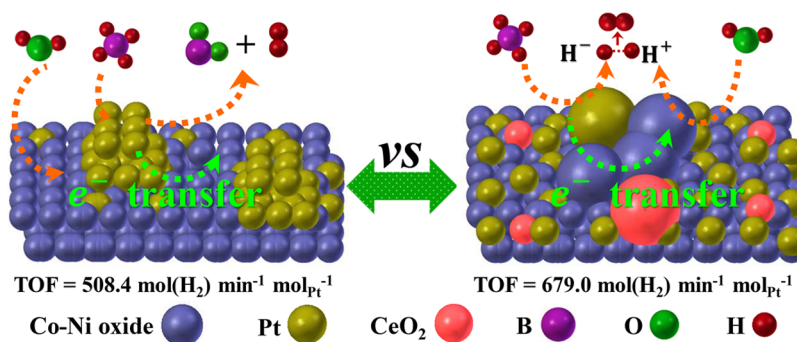


Figure 5. Catalytic mechanism diagram of the Pt/Co₇Ni₂O_x and Pt/CeO₂-Co₇Ni₂O_x hybrid catalysts for H₂ generation by hydrolysis of NaBH₄ solution.

(Figure S12). The specific H₂ evolution rate of Pt/CeO₂-Co₇Ni₂O_x in Figure 4b is much higher than that of Pt/Co₇Ni₂O_x. The different catalytic behaviors with and without CeO₂ was interpreted by the activation energy, and the time-dependent H₂ evolution activity was evaluated for hydrolysis of alkalinized NaBH₄ at different temperatures. As shown in Figure 4c, the specific reaction rates (*k*) slowly increase with increasing the applied hydrolysis temperatures from 298 to 318 K for NaBH₄ hydrolysis. The activation energy of catalyst can be calculated by the Arrhenius equation: $k = A \cdot e^{-E_a/RT}$, where the *k* (L min⁻¹ g⁻¹) is the specific H₂ evolution rate, *E_a* is the activation energy (kJ mol⁻¹), *R* is the gas constant (8.314 J mol⁻¹ K⁻¹), and *T* is the applied solution temperature (K). According to the equation, the calculated activation energy of the Pt/CeO₂-Co₇Ni₂O_x hybrid catalyst is 44.7 kJ mol⁻¹ (see Figure 4d), which is apparently lower than 48.4 kJ mol⁻¹ of the

Pt/Co₇Ni₂O_x, as well as most values reported before (Table S3). Additionally, the slow deactivation of the catalysts as cycling should be ascribed to the coefficient of Pt-alloy agglomerations (Figure S13), the varied chemical state of components (Figure S14) and the adsorbed reaction by-products (e.g., BO₂⁻) on the active sites.⁵²

Catalytic Mechanism Analysis. The TOF value of Pt/CeO₂-Co₇Ni₂O_x catalyst is ca. 1.34-fold higher than that of the Pt/Co₇Ni₂O_x catalyst, as shown in Figure 5. The improved catalytic performance results from the introduction of CeO₂ that can produce more tiny Pt atomic clusters, giving rise to more grain boundaries between the Pt atomic clusters and transition metal oxides support; therefore, they can significantly enhance the catalytic capabilities of NaBH₄ hydrolysis via synergistic effect. In detail, the dissolved BH₄⁻ ions can be selectively adsorbed onto the Pt-alloy atomic clusters surface

due to the existence of a large number of vacant 5d orbitals in the hybrid catalyst, the high molar ratio of $[\text{BH}_4^-]/[\text{Pt}]$ can facilitate the broken of the chemical bonds of B–H of BH_4^- ions, generating negative charged H^- by electron transfer from BH_4^- ions through the structure of $\text{Pt}/\text{CeO}_2\text{-Co}_7\text{Ni}_2\text{O}_x$.^{27,52} And also, the coexistent $\text{Ce}^{4+}/\text{Ce}^{3+}$ redox couple in the hybrid material can help promote the electron transfer process (Figure S14). Meanwhile, the H–OH bonds of adsorbed H_2O molecules on the hydrophilic Ce–Co–Ni oxide could be weakened, thus favoring the formation of H_2 ($\text{H}^+ + \text{H}^- \rightarrow \text{H}_2$) by promoting the ionization of H_2O ($\text{H}_2\text{O} \leftrightarrow \text{H}^+ + \text{OH}^-$).^{31,53} Thus, the higher performances result from the synergetic effect of Pt-alloy atomic clusters and Ce–Co–Ni oxide support.

CONCLUSIONS

In summary, the CeO_2 tailored Pt-alloy atomic clusters on Ce–Co–Ni oxide support have been designed for highly efficient $\text{Pt}/\text{CeO}_2\text{-Co}_7\text{Ni}_2\text{O}_x$ hybrid catalyst by a facile reduction method. The molar ratio of Co/Ni, the role of CeO_2 , and loading effect of Pt were studied in detail for designing the desired catalyst. We find that the $\text{Pt}/\text{CeO}_2\text{-Co}_7\text{Ni}_2\text{O}_x$ catalyst can significantly enhance the catalytic ability of H_2 evolution from hydrolysis of alkalized NaBH_4 solution at room temperature. The high specific rate and TOF value for H_2 evolution were confirmed resulting from the synergistic effect between the tiny Pt-alloy atomic clusters and Ce–Co–Ni oxide support, which can adsorb and break B–H bonds of BH_4^- and weaken H–O bonds of H_2O via electron transfer effect to generate H_2 . This work develops an efficient strategy to design a highly active and robust catalyst for H_2 generation on hydrolysis of NaBH_4 in which the catalytic reaction mechanism was discussed, and we postulate it is applicable in other fields.

ASSOCIATED CONTENT

Supporting Information

The Supporting Information is available free of charge on the ACS Publications website at DOI: 10.1021/acssuschemeng.8b00061.

More details on characterization of our synthesized materials and their electrocatalytic performance data; additional TEM, SEM, EDS, XPS, ICP-AES, and electrocatalytic performance data (PDF)

AUTHOR INFORMATION

Corresponding Authors

*X. Yang. E-mail: xiulin.yang@kaust.edu.sa.

*Y. Zhao. E-mail: yanchunzhao@aliyun.com.

*J. Ming. E-mail: jun.ming@ciac.ac.cn.

ORCID

Jun Ming: 0000-0001-9561-5718

Xiulin Yang: 0000-0003-2642-4963

Notes

The authors declare no competing financial interest.

ACKNOWLEDGMENTS

This work has been supported by the National Natural Science Foundation of China (21363003, 21165004, 21163002), Natural Science Foundation of Guangxi Province (2014GXNSFGA118008, 2014GXNSFFA118003), BAGUI scholar program (2014A001), and Project of Talents Highland of Guangxi Province.

REFERENCES

- (1) Yu, Y.; Zhang, Z.; Yin, X.; Kvit, A.; Liao, Q.; Kang, Z.; Yan, X.; Zhang, Y.; Wang, X. Enhanced photoelectrochemical efficiency and stability using a conformal TiO_2 film on a black silicon photoanode. *Nat. Energy* **2017**, *2*, 17045.
- (2) Santos, D. M. F.; Sequeira, C. A. C. Sodium borohydride as a fuel for the future. *Renewable Sustainable Energy Rev.* **2011**, *15* (8), 3980.
- (3) Yang, X.; Lu, A.-Y.; Zhu, Y.; Min, S.; Hedhili, M. N.; Han, Y.; Huang, K.-W.; Li, L.-J. Rague-Like FeP Nanocrystal Assembly on Carbon Cloth: An Exceptionally Efficient and Stable Cathode for Hydrogen Evolution. *Nanoscale* **2015**, *7* (25), 10974.
- (4) Ouyang, L.; Chen, W.; Liu, J.; Felderhoff, M.; Wang, H.; Zhu, M. Enhancing the Regeneration Process of Consumed NaBH_4 for Hydrogen Storage. *Adv. Energy Mater.* **2017**, *7* (19), 1700299.
- (5) Tan, Y.; Yu, X. Chemical regeneration of hydrogen storage materials. *RSC Adv.* **2013**, *3* (46), 23879.
- (6) Demirci, U. B.; Miele, P. Sodium borohydride versus ammonia borane, in hydrogen storage and direct fuel cell applications. *Energy Environ. Sci.* **2009**, *2* (6), 627.
- (7) Yan, J.-M.; Zhang, X.-B.; Akita, T.; Haruta, M.; Xu, Q. One-Step Seeding Growth of Magnetically Recyclable Au@Co Core–Shell Nanoparticles: Highly Efficient Catalyst for Hydrolytic Dehydrogenation of Ammonia Borane. *J. Am. Chem. Soc.* **2010**, *132* (15), 5326.
- (8) Metin, Ö.; Mazumder, V.; Özkaz, S.; Sun, S. Monodisperse Nickel Nanoparticles and Their Catalysis in Hydrolytic Dehydrogenation of Ammonia Borane. *J. Am. Chem. Soc.* **2010**, *132* (5), 1468.
- (9) Durano, M. M.; Tamboli, A. H.; Kim, H. Cobalt oxide synthesized using urea precipitation method as catalyst for the hydrolysis of sodium borohydride. *Colloids Surf., A* **2017**, *520*, 355.
- (10) Lin, K.-Y. A.; Chang, H.-A. Efficient hydrogen production from NaBH_4 hydrolysis catalyzed by a magnetic cobalt/carbon composite derived from a zeolitic imidazolate framework. *Chem. Eng. J.* **2016**, *296*, 243.
- (11) Kahri, H.; Flaud, V.; Touati, R.; Miele, P.; Demirci, U. B. Reaction intermediate/product-induced segregation in cobalt-copper as the catalyst for hydrogen generation from the hydrolysis of sodium borohydride. *RSC Adv.* **2016**, *6* (104), 102498.
- (12) Wang, Y.; Lu, Y.; Wang, D.; Wu, S.; Cao, Z.; Zhang, K.; Liu, H.; Xin, S. Hydrogen generation from hydrolysis of sodium borohydride using nanostructured NiB catalysts. *Int. J. Hydrogen Energy* **2016**, *41* (36), 16077.
- (13) Wang, Y.; Shen, Y.; Qi, K.; Cao, Z.; Zhang, K.; Wu, S. Nanostructured cobalt–phosphorous catalysts for hydrogen generation from hydrolysis of sodium borohydride solution. *Renewable Energy* **2016**, *89*, 285.
- (14) Liu, T.; Wang, K.; Du, G.; Asiri, A. M.; Sun, X. Self-supported CoP nanosheet arrays: a non-precious metal catalyst for efficient hydrogen generation from alkaline NaBH_4 solution. *J. Mater. Chem. A* **2016**, *4* (34), 13053.
- (15) Muir, S. S.; Chen, Z.; Wood, B. J.; Wang, L.; Lu, G. Q.; Yao, X. New electroless plating method for preparation of highly active Co–B catalysts for NaBH_4 hydrolysis. *Int. J. Hydrogen Energy* **2014**, *39* (1), 414.
- (16) Tang, C.; Zhang, R.; Lu, W.; He, L.; Jiang, X.; Asiri, A. M.; Sun, X. Fe-Doped CoP Nanoarray: A Monolithic Multifunctional Catalyst for Highly Efficient Hydrogen Generation. *Adv. Mater.* **2017**, *29* (2), 1602441.
- (17) Tomboc, G. R. M.; Tamboli, A. H.; Kim, H. Synthesis of Co_3O_4 macrocubes catalyst using novel chitosan/urea template for hydrogen generation from sodium borohydride. *Energy* **2017**, *121*, 238.
- (18) Sahiner, N.; Yasar, A. O.; Aktas, N. Metal-free pyridinium-based polymeric ionic liquids as catalyst for H_2 generation from NaBH_4 . *Renewable Energy* **2017**, *101*, 1005.
- (19) Sahiner, N.; Demirci, S. Natural microgranular cellulose as alternative catalyst to metal nanoparticles for H_2 production from NaBH_4 methanolysis. *Appl. Catal., B* **2017**, *202*, 199.
- (20) Şahin, Ö.; Karakaş, D. E.; Kaya, M.; Saka, C. The effects of plasma treatment on electrochemical activity of Co–B–P catalyst for

- hydrogen production by hydrolysis of NaBH_4 . *J. Energy Inst.* **2017**, *90* (3), 466.
- (21) Li, Z.; Wang, L.; Zhang, Y.; Xie, G. Properties of $\text{CuCoP}/\gamma\text{-Al}_2\text{O}_3$ catalysts for efficient hydrogen generation by hydrolysis of alkaline NaBH_4 solution. *Int. J. Hydrogen Energy* **2017**, *42* (9), 5749.
- (22) Jadhav, A. R.; Bandal, H. A.; Kim, H. NiCo_2O_4 hollow sphere as an efficient catalyst for hydrogen generation by NaBH_4 hydrolysis. *Mater. Lett.* **2017**, *198*, 50.
- (23) Cui, L.; Xu, Y.; Niu, L.; Yang, W.; Liu, J. Monolithically integrated CoP nanowire array: An on/off switch for effective on-demand hydrogen generation via hydrolysis of NaBH_4 and NH_3BH_3 . *Nano Res.* **2017**, *10* (2), 595.
- (24) Zhang, X.-B.; Yan, J.-M.; Han, S.; Shioyama, H.; Xu, Q. Magnetically Recyclable Fe@Pt Core–Shell Nanoparticles and Their Use as Electrocatalysts for Ammonia Borane Oxidation: The Role of Crystallinity of the Core. *J. Am. Chem. Soc.* **2009**, *131* (8), 2778.
- (25) Lale, A.; Wasan, A.; Kumar, R.; Miele, P.; Demirci, U. B.; Bernard, S. Organosilicon polymer-derived mesoporous 3D silicon carbide, carbonitride and nitride structures as platinum supports for hydrogen generation by hydrolysis of sodium borohydride. *Int. J. Hydrogen Energy* **2016**, *41* (34), 15477.
- (26) Irum, M.; Zaheer, M.; Friedrich, M.; Kempe, R. Mesoporous silica nanosphere supported platinum nanoparticles (Pt@MSN): one-pot synthesis and catalytic hydrogen generation. *RSC Adv.* **2016**, *6* (13), 10438.
- (27) Hung, T.-F.; Kuo, H.-C.; Tsai, C.-W.; Chen, H. M.; Liu, R.-S.; Weng, B.-J.; Lee, J.-F. An alternative cobalt oxide-supported platinum catalyst for efficient hydrolysis of sodium borohydride. *J. Mater. Chem.* **2011**, *21* (32), 11754.
- (28) Liu, Z.; Guo, B.; Chan, S. H.; Tang, E. H.; Hong, L. Pt and Ru dispersed on LiCoO_2 for hydrogen generation from sodium borohydride solutions. *J. Power Sources* **2008**, *176* (1), 306.
- (29) Nunes, H. X.; Ferreira, M. J. F.; Rangel, C. M.; Pinto, A. M. F. R. Hydrogen generation and storage by aqueous sodium borohydride (NaBH_4) hydrolysis for small portable fuel cells (H_2 -PEMFC). *Int. J. Hydrogen Energy* **2016**, *41* (34), 15426.
- (30) Wei, L.; Yuan, Z. Effects of Ag doping on the catalytic performance of Co-B NPs for hydrolysis of alkaline sodium borohydride solution. *AIP Conf. Proc.* **2016**, *1794* (1), 020004.
- (31) Jiao, C.; Huang, Z.; Wang, X.; Zhang, H.; Lu, L.; Zhang, S. Synthesis of Ni/Au/Co trimetallic nanoparticles and their catalytic activity for hydrogen generation from alkaline sodium borohydride aqueous solution. *RSC Adv.* **2015**, *5* (43), 34364.
- (32) Wang, H.-L.; Yan, J.-M.; Wang, Z.-L.; O, S.-I.; Jiang, Q. Highly efficient hydrogen generation from hydrous hydrazine over amorphous $\text{Ni}_{0.9}\text{Pt}_{0.1}/\text{Ce}_2\text{O}_3$ nanocatalyst at room temperature. *J. Mater. Chem. A* **2013**, *1* (47), 14957.
- (33) Wang, L.; Huang, L.; Jiao, C.; Huang, Z.; Liang, F.; Liu, S.; Wang, Y.; Zhang, H. Preparation of Rh/Ni Bimetallic Nanoparticles and Their Catalytic Activities for Hydrogen Generation from Hydrolysis of KBH_4 . *Catalysts* **2017**, *7* (4), 125.
- (34) Kang, J.-X.; Chen, T.-W.; Zhang, D.-F.; Guo, L. PtNiAu trimetallic nanoalloys enabled by a digestive-assisted process as highly efficient catalyst for hydrogen generation. *Nano Energy* **2016**, *23*, 145.
- (35) Zhao, Y.; Yang, X.; Zhan, L.; Ou, S.; Tian, J. High electrocatalytic activity of PtRu nanoparticles supported on starch-functionalized multi-walled carbon nanotubes for ethanol oxidation. *J. Mater. Chem.* **2011**, *21* (12), 4257.
- (36) Zhao, Y.; Wang, F.; Tian, J.; Yang, X.; Zhan, L. Preparation of Pt/CeO₂/HCSs anode electrocatalysts for direct methanol fuel cells. *Electrochim. Acta* **2010**, *55* (28), 8998.
- (37) She, Y.; Lu, Z.; Fan, W.; Jewell, S.; Leung, M. K. H. Facile preparation of PdNi/rGO and its electrocatalytic performance towards formic acid oxidation. *J. Mater. Chem. A* **2014**, *2* (11), 3894.
- (38) Peng, X.; Chen, D.; Yang, X.; Wang, D.; Li, M.; Tseng, C.-C.; Panneerselvam, R.; Wang, X.; Hu, W.; Tian, J.; Zhao, Y. Microwave-Assisted Synthesis of Highly Dispersed PtCu Nanoparticles on Three-Dimensional Nitrogen-Doped Graphene Networks with Remarkably Enhanced Methanol Electrooxidation. *ACS Appl. Mater. Interfaces* **2016**, *8* (49), 33673.
- (39) Bruix, A.; Lykhach, Y.; Matolinová, I.; Neitzel, A.; Skála, T.; Tsud, N.; Vorokhta, M.; Stetsovych, V.; Ševčíková, K.; Mysliveček, J.; Fiala, R.; Václavů, M.; Prince, K. C.; Bruyère, S.; Potin, V.; Illas, F.; Matolin, V.; Libuda, J.; Neyman, K. M. Maximum Noble-Metal Efficiency in Catalytic Materials: Atomically Dispersed Surface Platinum. *Angew. Chem., Int. Ed.* **2014**, *53* (39), 10525.
- (40) Zhao, Y.; Yang, X.; Tian, J.; Wang, F.; Zhan, L. Methanol electro-oxidation on Ni@Pd core-shell nanoparticles supported on multi-walled carbon nanotubes in alkaline media. *Int. J. Hydrogen Energy* **2010**, *35* (8), 3249.
- (41) Feng, J.-X.; Ye, S.-H.; Xu, H.; Tong, Y.-X.; Li, G.-R. Design and Synthesis of FeOOH/CeO₂ Heterolayered Nanotube Electrocatalysts for the Oxygen Evolution Reaction. *Adv. Mater.* **2016**, *28* (23), 4698.
- (42) Yang, X.; Li, H.; Lu, A.-Y.; Min, S.; Idriss, Z.; Hedhili, M. N.; Huang, K.-W.; Idriss, H.; Li, L.-J. Highly acid-durable carbon coated Co_3O_4 nanoarrays as efficient oxygen evolution electrocatalysts. *Nano Energy* **2016**, *25*, 42.
- (43) Biesinger, M. C.; Payne, B. P.; Grosvenor, A. P.; Lau, L. W. M.; Gerson, A. R.; Smart, R. S. C. Resolving surface chemical states in XPS analysis of first row transition metals, oxides and hydroxides: Cr, Mn, Fe, Co and Ni. *Appl. Surf. Sci.* **2011**, *257* (7), 2717.
- (44) Bai, Y.; Wu, C.; Wu, F.; Yi, B. Carbon-supported platinum catalysts for on-site hydrogen generation from NaBH_4 solution. *Mater. Lett.* **2006**, *60* (17), 2236.
- (45) Yao, Q.; Shi, W.; Feng, G.; Lu, Z.-H.; Zhang, X.; Tao, D.; Kong, D.; Chen, X. Ultrafine Ru nanoparticles embedded in SiO_2 nanospheres: Highly efficient catalysts for hydrolytic dehydrogenation of ammonia borane. *J. Power Sources* **2014**, *257*, 293.
- (46) Akbayrak, S.; Kaya, M.; Volkan, M.; Özkur, S. Ruthenium(0) nanoparticles supported on magnetic silica coated cobalt ferrite: Reusable catalyst in hydrogen generation from the hydrolysis of ammonia-borane. *J. Mol. Catal. A: Chem.* **2014**, *394*, 253.
- (47) Akbayrak, S.; Kaya, M.; Volkan, M.; Özkur, S. Palladium(0) nanoparticles supported on silica-coated cobalt ferrite: A highly active, magnetically isolable and reusable catalyst for hydrolytic dehydrogenation of ammonia borane. *Appl. Catal., B* **2014**, *147*, 387.
- (48) Chen, J.; Lu, Z.-H.; Wang, Y.; Chen, X.; Zhang, L. Magnetically recyclable $\text{Ag}/\text{SiO}_2\text{-CoFe}_2\text{O}_4$ nanocomposite as a highly active and reusable catalyst for H_2 production. *Int. J. Hydrogen Energy* **2015**, *40* (14), 4777.
- (49) Wang, L.; Li, H.; Zhang, W.; Zhao, X.; Qiu, J.; Li, A.; Zheng, X.; Hu, Z.; Si, R.; Zeng, J. Supported Rhodium Catalysts for Ammonia–Borane Hydrolysis: Dependence of the Catalytic Activity on the Highest Occupied State of the Single Rhodium Atoms. *Angew. Chem., Int. Ed.* **2017**, *56* (17), 4712.
- (50) Zhang, J.; Chen, C.; Chen, S.; Hu, Q.; Gao, Z.; Li, Y.; Qin, Y. Highly dispersed Pt nanoparticles supported on carbon nanotubes produced by atomic layer deposition for hydrogen generation from hydrolysis of ammonia borane. *Catal. Sci. Technol.* **2017**, *7* (2), 322.
- (51) Zhang, M.; Liu, L.; He, T.; Li, Z.; Wu, G.; Chen, P. Microporous Crystalline $\gamma\text{-Al}_2\text{O}_3$ Replicated from Microporous Covalent Triazine Framework and Its Application as Support for Catalytic Hydrolysis of Ammonia Borane. *Chem. - Asian J.* **2017**, *12* (4), 470.
- (52) Bandal, H. A.; Jadhav, A. R.; Kim, H. Cobalt impregnated magnetite-multiwalled carbon nanotube nanocomposite as magnetically separable efficient catalyst for hydrogen generation by NaBH_4 hydrolysis. *J. Alloys Compd.* **2017**, *699*, 1057.
- (53) Demirci, U. B.; Miele, P. Reaction mechanisms of the hydrolysis of sodium borohydride: A discussion focusing on cobalt-based catalysts. *C. R. Chim.* **2014**, *17* (7), 707.